



# CHORUS

This is the accepted manuscript made available via CHORUS. The article has been published as:

## Interface symmetry and spin control in topological-insulator–semiconductor heterostructures

Mahmoud M. Asmar, Daniel E. Sheehy, and Ilya Vekhter

Phys. Rev. B **95**, 241115 — Published 29 June 2017

DOI: [10.1103/PhysRevB.95.241115](https://doi.org/10.1103/PhysRevB.95.241115)

# Interface symmetry and spin control in topological insulator-semiconductor heterostructures

Mahmoud M. Asmar, Daniel E. Sheehy, and Ilya Vekhter

*Department of Physics and Astronomy, Louisiana State University, Baton Rouge, LA 70803-4001*

(Dated: November 14, 2016)

Heterostructures combining topological and non-topological materials constitute the next frontier in the effort to incorporate topological insulators (TIs) into electronic devices. We show that the properties of the interface states appearing at the boundary between a topologically-trivial semiconductor (SE) and a TI are controlled by the lowering of the interface symmetry due to the presence of the SE. For the [111]-grown heterostructure, SE-TI interface states exhibit elliptical contours of constant energy and complex spin textures with broken helicity, in contrast to the well-studied helical Dirac surface states. We derive a general effective Hamiltonian for SE-TI junctions, and propose experimental signatures such as an out of plane spin accumulation under a transport current and the opening of a spectral gap that depends on the direction of an applied in-plane magnetic field.

PACS numbers:

*Introduction.* The control of topologically-protected metallic interface states [1–3] in heterostructures containing topological insulators (TIs) along with materials such as semiconductors (SE) [4–6], superconductors [7–9], or magnets [10, 11], yields new functionalities ranging from spintronics [12–14] to thermoelectrics [15], to quantum computing [16]. It is often assumed that the main low-energy features of the interface states are identical to those of the surface states at a vacuum termination of a TI. For the [111] crystal orientation of  $\text{Bi}_2\text{Se}_3$ , the characteristic isotropic Dirac dispersion and helical spin-momentum locking of the states at the surface [1, 2, 17–20], are commonly ascribed to the interface states.

We show that these features of the TI surface states require protection by spatial symmetries that can be broken at interfaces. We consider all time-reversal (TR) invariant interface potentials, and derive the most general low-energy Hamiltonian for SE-TI interfaces. We find that, in contrast to the surface states of TIs [21, 22], the interface states exhibit broken helicity, with spins rotating out of the plane of the interface, and broken in-plane rotational symmetry leading to an elliptical Dirac-like energy spectrum, as summarized in Fig. 1. As a result, an in-plane Zeeman field may open a field-orientation-dependent gap in the spectrum, in contrast to its effect on the surface [23]. In addition, under an in-plane transport current, the spin accumulation at interfaces can have an out-of-plane component.

*Symmetries of a SE-TI junction.* We consider a flat planar [111]-oriented interface,  $z = 0$ , between a semi-infinite three-dimensional TI and a topologically-trivial SE, see Fig. 1 (inset). For a vacuum termination, the two-dimensional states near  $z = 0$  [24–26] are described by a Dirac Hamiltonian in spin space,

$$H_D = v(\boldsymbol{\sigma} \times \mathbf{p})_z, \quad (1)$$

where  $\mathbf{p} = (p_x, p_y)$  is the in-plane momentum,  $v$  is the effective velocity ( $\hbar = 1$ ) and  $\boldsymbol{\sigma}$  is a vector of the Pauli

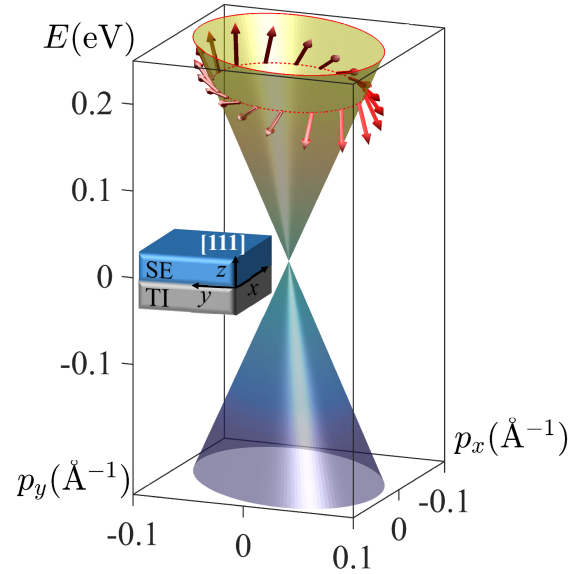


FIG. 1: Energy dispersion and spin texture (arrows) of the topological state at a SE-TI interface [38]. The interface potentials are  $u_3 = u_4 = 0.71A_1$  and  $u_5 = 0.1A_2$ . For all numerical work  $A_1 = 2.26 \text{ eV}\text{\AA}$ ,  $A_2 = 3.33 \text{ eV}\text{\AA}$ ,  $B_1 = -6.86 \text{ eV}\text{\AA}^2$ ,  $B_2 = -44.5 \text{ eV}\text{\AA}^2$ , and  $M = -m = 0.28 \text{ eV}$ . [26] Note the ellipticity of the constant energy contours, and the out of plane tilt of the spins. Inset: Geometry of the SE-TI junction.

matrices. The eigenstates of  $H_D$  have an isotropic linear dispersion,  $E(\mathbf{p}) = \pm v|\mathbf{p}|$ , with rotational symmetry around the  $\hat{z}$  axis,  $C_\infty$ . Since  $H_D$  commutes with the helicity operator,  $\hat{h} = (\boldsymbol{\sigma} \times \mathbf{p})_z/p$ , the eigenstates are helical, with the spin expectation value in the plane and perpendicular to  $\mathbf{p}$ . These are the symmetries of bulk TI materials, such as  $\text{Bi}_2\text{Se}_3$  [24], in the low energy limit for the appropriate crystal face [19, 20]. Thus, Eq. (1) assumes that no additional symmetries are broken by the interface [27–29].

Real SE-TI interfaces are likely to have lower symmetry than the bulk [30, 31], strongly modifying electronic properties. The most general (topologically equivalent to

Irrep	E	C <sub>2</sub>	$\hat{\sigma}_{\mathbf{e}}$	$\hat{\sigma}_{\bar{\mathbf{e}}}$	Term in $H_I$	Term in $\hat{U}$
$\mathcal{A}_1$	1	1	1	1	$\Delta, v_1, v_4$	$u_0, u_1, u_2$
$\mathcal{A}_2$	1	1	-1	-1	$v_2, v_6$	$u_5$
$\mathcal{B}_1$	1	-1	1	-1	$v_5$	None
$\mathcal{B}_2$	1	-1	-1	1	$v_3$	$u_3, u_4$

TABLE I: Character table of the irreducible representations of  $C_{2v}$ . Here, E is the identity operation,  $C_2$  is two-fold rotation, and  $\hat{\sigma}_{\mathbf{e}}$  and  $\hat{\sigma}_{\bar{\mathbf{e}}}$  are mirror reflections with respect to the  $\mathbf{e}$ - $\hat{z}$  and  $\bar{\mathbf{e}}$ - $\hat{z}$  planes, respectively. The third and fourth columns classify the symmetries of the interface Hamiltonian, Eq. (3), and the interface potential  $\hat{U}$ , Eq. (6), respectively.

$H_D$ ) linear in  $\mathbf{p}$  Hamiltonian that is invariant under TR,

$$H_I = \sigma_0 \Delta + \sum_{m=x,y,z} \sum_{n=x,y} c_{mn} \sigma_m p_n, \quad (2)$$

is characterized by seven real parameters: An overall energy shift  $\Delta$ , and the coefficients  $c_{mn}$ . Here  $\sigma_0 \equiv \mathbb{1}_{2 \times 2}$ .  $H_I$  has a much lower symmetry than  $H_D$ . Continuous rotational symmetry around the  $\hat{z}$  axis,  $C_\infty$ , is absent. The helicity is also broken. However,  $H_I$  is particle-hole symmetric (relative to the shift  $\Delta$ ) since the anticommutator  $\{\boldsymbol{\sigma} \cdot \mathbf{m}, H_I - \sigma_0 \Delta\} = 0$  for the vector  $\mathbf{m} = (c_{yx}c_{zy} - c_{yy}c_{zx}, c_{xy}c_{zx} - c_{xx}c_{zy}, c_{xx}c_{yy} - c_{xy}c_{yx})$ . Moreover, the spins of all the eigenstates of  $H_I$  are in the plane normal to  $\mathbf{m}$  [32].

For a [111] surface termination,  $\mathbf{m} \parallel \hat{z}$ , maintaining the  $C_\infty$  symmetry. When  $\mathbf{m}$  points away from the  $z$ -axis, the symmetry group is reduced, and depends on the spin-orbit structure of the interface potential. We now introduce  $\mathbf{e}$ , a vector in the  $x$ - $y$  plane (defined below by the interface potentials), and  $\bar{\mathbf{e}} = \hat{z} \times \mathbf{e}$ , with which we can rewrite Eq. (2) as [32]:

$$H_I = \Delta \sigma_0 + v_1 (\boldsymbol{\sigma} \times \mathbf{p})_z + v_2 \boldsymbol{\sigma} \cdot \mathbf{p} + v_3 \sigma_z \mathbf{p} \cdot \mathbf{e} \quad (3) \\ + v_4 (\boldsymbol{\sigma} \cdot \bar{\mathbf{e}}) (\mathbf{p} \cdot \mathbf{e}) + v_5 \sigma_z (\mathbf{p} \cdot \bar{\mathbf{e}}) + v_6 (\boldsymbol{\sigma} \cdot \mathbf{e}) (\mathbf{p} \cdot \mathbf{e}).$$

The advantage of Eq. (3) is that each term belongs to a particular irreducible representation (irrep) of the  $C_{2v}$  group, as listed in Table I. The spin structure of the eigenstates of  $H_I$  depends on the parameters  $v_i$ , which we now compute within a specific model.

*Model of a SE-TI junction.* We model the interface by the Hamiltonian

$$H = H_{\text{TI}} \Theta(-z) + H_{\text{SE}} \Theta(z) + \hat{U} \delta(z). \quad (4)$$

Here  $H_{\text{TI}}$  ( $H_{\text{SE}}$ ) describes a bulk topological insulator (semiconductor) at  $z < 0$  ( $z > 0$ ), and  $\Theta(z)$  is the step function. The last term describes the interface potential, with the delta-function simplifying calculations without loss of generality.

We take  $H_{\text{TI}}$  in the form suggested for  $\text{Bi}_2\text{Se}_3$  [26], written as a  $4 \times 4$  matrix in the basis of column vectors

$\psi = (\psi_{+\uparrow}, \psi_{-\uparrow}, \psi_{+\downarrow}, \psi_{-\downarrow})^T$ , where the subscripts  $\pm$  ( $\uparrow, \downarrow$ ) refer to parity (spin),

$$H_{\text{TI}} = \sigma_0 \otimes [\tau_z (M - B_1 p_z^2 - B_2 p^2) + A_1 \tau_y p_z] \\ + A_2 (\boldsymbol{\sigma} \times \mathbf{p})_z \otimes \tau_x. \quad (5)$$

Here  $A_i, B_i$ , ( $i = 1, 2$ ) are material-dependent constants,  $M > 0$  determines the TI bulk band gap,  $\tau_i$  is the Pauli matrix in the parity space, and  $\otimes$  denotes a direct product. Since the relative sign of  $M$  and  $B_i$  determines the topological properties, we take  $H_{\text{SE}}$  to differ from  $H_{\text{TI}}$  only by the sign of mass parameter ( $M \rightarrow -m < 0$ ). Note that both  $H_{\text{TI}}$  and  $H_{\text{SE}}$  have particle-hole symmetry since, for  $\mathcal{P} = \sigma_z \otimes \tau_x$ , we have  $\{\mathcal{P}, H_{\text{TI/SE}}\} = 0$ .

The symmetry of the matrix  $\hat{U}$  controls the nature of the interface states, while the strength of the symmetry-breaking terms depends on the microscopic parameters of  $H$ . Requiring TR invariance dictates

$$\hat{U} = \sigma_0 \otimes [u_0 \tau_0 + u_1 \tau_z + u_2 \tau_x] + [u_3 \sigma_x + u_4 \sigma_y + u_5 \sigma_z] \otimes \tau_y. \quad (6)$$

This formalism generally captures the physics of semiconducting interfaces in the  $\mathbf{k} \cdot \mathbf{p}$  methods [33–37]. For  $\text{Bi}_2\text{Se}_3$  the even (odd) parity wave functions originate from Bi (Se)  $p_z$ -orbitals [26]. Hence  $u_0 \pm u_1$  describe charging on the Bi and Se sites respectively, while parity-mixing  $u_2$  may arise from interdiffusion on Se sites. The interface spin-orbit term  $u_5$  (respecting rotations) may come from a staggered potential involving heavy ions on TI or SE side, such as buckling, while  $u_{3,4}$  appear from incommensurability or strain (intrinsic or extrinsic) at the interface. Due to spin-orbit coupling, lowering spin symmetry breaks real-space rotations as well, and  $u_{3,4}$  define the vector  $\mathbf{e}$  according to

$$u_3 \sigma_x + u_4 \sigma_y = q \mathbf{e} \cdot \boldsymbol{\sigma}, \quad q = \sqrt{u_3^2 + u_4^2}. \quad (7)$$

Notably, as seen in Table I, the terms in  $\hat{U}$  can also be classified according to the  $C_{2v}$  point group. We now derive Eq. (3) from the Hamiltonian, Eq. (4).

*Effective Interface Hamiltonian.* Using Eq. (4) we determine the energies,  $E_i$ , and normalized eigenfunctions,  $|\Psi_i\rangle$ , of the states localized at the interface, and form the matrix representation of the interface Hamiltonian  $H_I = \sum_i E_i |\Psi_i\rangle \langle \Psi_i|$ . The wave functions on each side are the linear combinations of the solutions of  $H_{\text{SE}}$  and  $H_{\text{TI}}$  respectively, chosen to decay away from the interface. The boundary conditions for the continuity of the wave function and the discontinuity of its derivative at  $z = 0$  give a set of 8 equations for the coefficients of this linear combination, [32]  $\mathcal{B} \mathbf{x} = 0$  where  $\mathcal{B}$  is given by the parameters of  $H$ . The roots of  $\det \mathcal{B} = 0$  give  $E(\mathbf{p})$ , while the eigenvectors  $\mathbf{x}_E(\mathbf{p})$  determine the eigenfunctions. [49]

To derive an analytic form of the interface Hamiltonian valid at low energies, we evaluate  $\det \mathcal{B}$  to second order in  $E$  and  $\mathbf{p}$ . The resulting lengthy expressions directly give

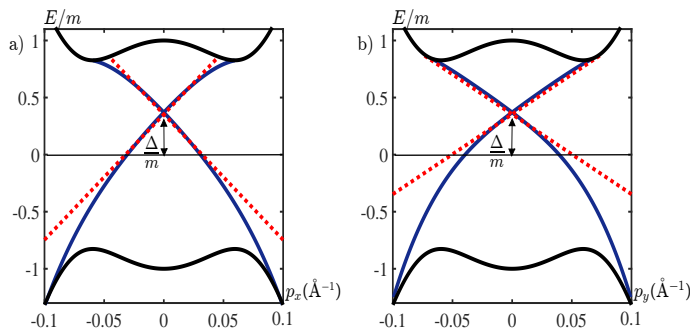


FIG. 2: Numerical (solid lines) and approximate analytical (dashed lines) dispersion curves along the  $p_y = 0$ , (a), and  $p_x = 0$ , (b), directions [38]. The interface potentials are  $u_0 = 0.6A_2$ ,  $u_2 = -0.3A_2$ ,  $u_1 = 0.1A_2$ ,  $u_5 = 0.15A_2$ ,  $q = 0.9A_2$  and  $\phi = 0$ .

the the coefficients  $\Delta$  and  $v_i$  of Eq. (3) in terms of the parameters of both the bulk Hamiltonian and the interface potential  $\hat{U}$  [32]. Fig. 2 shows excellent agreement of the dispersion obtained in this linearized approximation with the numerical solution, and clearly demonstrates broken rotational symmetry of the spectrum.

Only two of the four components of the eigenstates  $\Psi$  are linearly independent (corresponding to different spin eigenstates, but mixed parity) [32]. As a result, the Hamiltonian has only four non-vanishing components and takes the  $2 \times 2$  form of Eq. (3). According to Table I no part of the interface potential in our model belongs to the  $\mathcal{B}_1$  irrep, and hence  $v_5 = 0$ .

*Representative results.* Since the interface is characterized by six coefficients,  $u_i$  in Eq. (6), there is a large parameter space to explore, and we focus on conceptually important cases. First, if either  $u_i \rightarrow \infty$  or  $|m| \rightarrow \infty$  (an impenetrable interface) we recover the Dirac Hamiltonian of the [111] face termination [32]. However, the asymptotic approach to these limits is very slow [32], so that the results below are relevant to all real heterostructures.

The  $\mathcal{A}_1$  terms  $u_0$ ,  $u_1$ , and  $u_2$  do not lower the symmetry of the crystal interface, so that for our [111] choice [39]

$$H_I = \Delta\sigma_0 + v_1(\boldsymbol{\sigma} \times \mathbf{p})_z. \quad (8)$$

Since  $\{u_1\sigma_0 \otimes \tau_z, \mathcal{P}\} = 0$ , the shift  $\Delta$  is induced by  $u_0$  and  $u_2$ , with the coefficients, and  $v_1$  renormalization, that depend on microscopic details [32].

Remarkable differences appear for other cases. Perfect helicity is broken for TR-invariant, but spin-dependent,  $\hat{U}$ . Consider  $\hat{U} = u_5\sigma_z \otimes \tau_y$  in the  $\mathcal{A}_2$  irrep, with all other  $u_i = 0$ . Since  $\{\mathcal{P}, H\} = 0$ , there is no energy shift,  $\Delta = 0$ . As  $C_\infty$  is preserved,  $v_4 = v_6 = 0$  also, yielding

$$H_I = v_1(\boldsymbol{\sigma} \times \mathbf{p})_z + v_2\boldsymbol{\sigma} \cdot \mathbf{p} = v'(\boldsymbol{\sigma} \times \mathbf{p})_z e^{i\sigma_z\beta}. \quad (9)$$

The two terms together lead to the Dirac Hamiltonian with the renormalized velocity,  $v' = \sqrt{v_1^2 + v_2^2}$ , and a

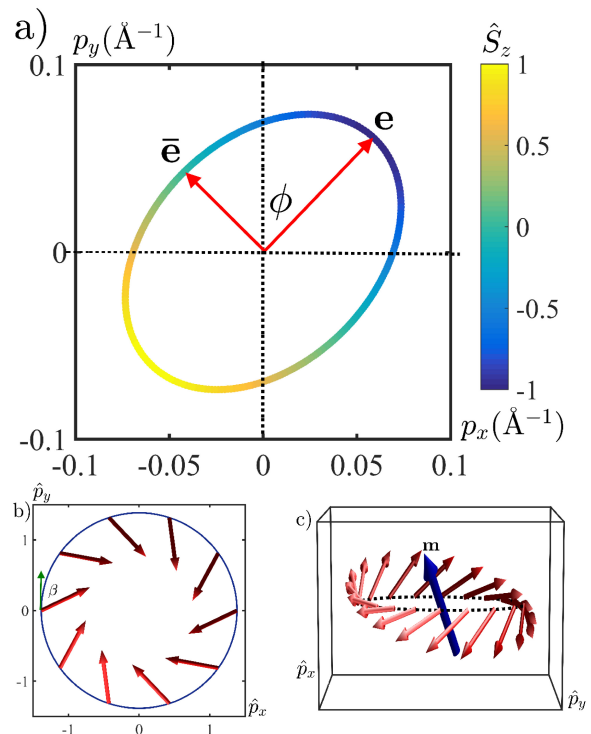


FIG. 3: Constant energy surface and spin texture of the interface states. Panel (a) shows the remaining twofold symmetry with the vectors  $\mathbf{e}$  and  $\bar{\mathbf{e}}$  along the semi-axes of the ellipse, see text. Color indicates the  $z$  component of the spin,  $\hbar\hat{S}_z/2 = \langle\sigma_z\rangle$  with  $E = 2meV$  and other parameters the same as in Fig.1. Panel (b): effect of broken helical symmetry due to the  $\mathcal{A}_2$  irrep potential  $u_5 = A_2$ . Panel (c): All the spins for  $E = 2meV$ , for  $q = 0.45A_2$  and  $\phi = \pi/4$  ( $u_3 = u_4 = 0.32A_2$ ) are normal to a vector  $\mathbf{m}$  described in text. Here  $\hat{\mathbf{p}} = A_2\mathbf{p}/E$ .

global spin rotation by  $\beta = \tan^{-1}(v_2/v_1)$  around the  $z$ -axis. The spins of the eigenstates stay in the plane, but are no longer normal to  $\mathbf{p}$ , see Fig. 3(b). The coefficient  $v_2$  (and  $\tan\beta$ ) is proportional to  $u_5$ .

The breaking of rotational symmetry requires  $u_{3,4} \neq 0$ , and we now consider this case, with all other  $u_i = 0$ . Then the  $C_2$  and one of the mirror symmetries are broken, see Table I, implying

$$H_I = v_1(\boldsymbol{\sigma} \times \mathbf{p})_z + v_3\sigma_z\mathbf{p} \cdot \mathbf{e} + v_4(\boldsymbol{\sigma} \cdot \bar{\mathbf{e}})(\mathbf{p} \cdot \mathbf{e}), \quad (10)$$

where  $v_1$ ,  $v_3$  and  $v_4$  depend on  $u_i$  [32]. The powers of  $\mathbf{e}$  in this expression correspond to the powers of  $q$  from Eq. (7), so that  $v_3 \propto q$ , while  $v_4 \propto q^2$ . The former induces a spin rotation around the  $\mathbf{e}$  axis, see Fig. 3(c), tilting the spins out of the plane of the interface. At the same time the constant energy contours stretch along the direction of the ( $\hat{U}$ -dependent) vector  $\mathbf{e}$ , and become elliptical, see Fig. 3(a).

Power counting, confirmed by detailed calculations, shows that  $v_6 \propto u_5q^2$  only appears in the presence of both  $\mathcal{A}_2$  and  $\mathcal{B}_2$  irrep terms of  $\hat{U}$ . While the expressions for  $v_i$  become complex when all  $u_i \neq 0$ , we confirmed that our conclusions remain valid over a wide parameter

range [32].

*Experimental Consequences.* We now contrast the experimental consequences of the anisotropic dispersion and unusual spin textures of the SE-TI interface states with the expected behavior of the Dirac surface states. First, for perfectly helical states, the application of a magnetic field parallel to the interface shifts the Dirac cone in momentum space, but does not change the spectrum or the helicity [23]. In contrast, if the spin of the interface state has an out-of-plane component, as for the SE-TI interfaces with the  $\mathcal{B}_2$  potential, Eq. (7), an in-plane field,  $\mathbf{B}$ , opens a spectral gap,  $\delta(\mathbf{B})$ .

If  $\mathbf{B}$  is at an angle  $\theta$  to the  $x$ -axis,  $\delta(\mathbf{B}) = 2|\mathbf{h} \cdot \widehat{\mathbf{m}}|$ , where  $\mathbf{h} = g\mu_B\mathbf{B}$ ,  $\widehat{\mathbf{m}} = \mathbf{m}/|\mathbf{m}|$ , and  $\mathbf{m}$  is the vector normal to the spins at the interface, given above. The gap is maximal for the field along (or opposite to) the in-plane projection of  $\mathbf{m}$ , and vanishes when  $\mathbf{B}$  is normal to that direction, see Fig. 4a). The spectrum remains gapless only for  $\mathbf{m} \parallel \hat{z}$ , not for a generic interface.

Second, from Eq. (3), the components  $j_i$  of the current operator are proportional to the spin density [14] along a direction that depends on the coefficients of  $H_I$ . Therefore, a transport current generates net spin magnetic moment.

For the usual helical surface states the direction of this moment is in the plane and normal to the current [12, 13]. Such an accumulation was observed experimentally [40–42]. We find that the spin structure depends on the interface. As discussed above, the  $u_5$  potential leads to an in-plane spin rotation (hence the net magnetic moment acquires a component along the current), while the  $u_3$  and  $u_4$  potentials rotate the spins out of the interface plane, leading to an accumulation of the  $z$ -component of the spin. This behavior is shown in Fig. 4b). A transport current parallel to the vector  $\mathbf{e}$  ( $\bar{\mathbf{e}}$ ) yields a spin polarization normal (parallel) to the interface. Importantly, accumulation of the spin component parallel to  $\mathbf{m}$  never occurs. An externally imposed strain [43, 44] breaks rotational symmetry, and is expected to induce the  $u_3$  and  $u_4$  terms, allowing control of the direction of the spin polarization.

*Discussion and Concluding Remarks* We derived the most general low-energy Hamiltonian, Eq. (3), that describes robust SE-TI interface states. While it is topologically equivalent to the Dirac Hamiltonian, it reflects lowering of the symmetry of the crystal face by the interface potentials, made relevant by the presence of a semiconductor (rather than vacuum).

Even for the most symmetric [111] heterostructure growth direction, only under special conditions are the interface states described by the helical Dirac Hamiltonian. In general such SE-TI interfaces exhibit an anisotropic energy dispersion, with the electron spin locked at an interface-dependent angle relative to the momentum, see Eq. (3). This result suggests that some of the properties of topological heterostructures may need to be

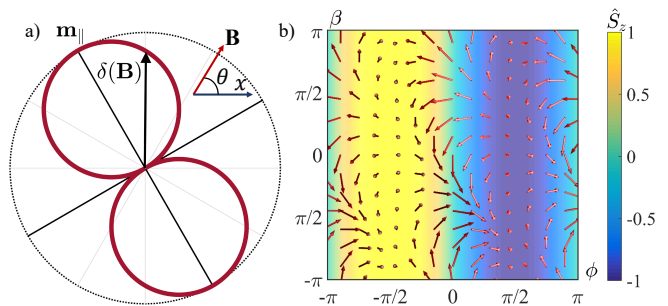


FIG. 4: Experimental consequences of the broken helicity and anisotropy of the Dirac cone. a) Polar plot of the gap generated by an in plane magnetic field as a function of the field direction.  $\mathbf{m}_{\parallel}$  is the in-plane projection of  $\mathbf{m}$ . b) Spin accumulation under transport current along the  $x$ -axis as a function of the in-plane helicity deviation angle,  $\beta$ , and the angle between the major semi-axis of the elliptical dispersion,  $\mathbf{e}$ , and the  $y$ -axis,  $\phi$ . Arrows and color indicate the spin orientation, and the out of plane component of spin respectively. The full  $z$ -axis polarization is achieved for current along  $\mathbf{e}$ , while for the current along  $\bar{\mathbf{e}}$  the magnetic moment is entirely in the plane. For panel b)  $q = 0.9A_2$ .

reanalysed.[7, 45–47]

First principles calculations are required to determine the values of the  $u_i$  for specific interfaces. In conventional semiconductor heterostructures the relaxation of atomic positions always leads to a lowering of the crystal symmetry to  $C_{2v}$  at the interface [30, 31]. Our analysis is consistent with this picture. Any dependence of the interface potential on the in-plane coordinates,  $x$  and  $y$  (e.g. due to buckling) gives higher order terms in  $p_{x,y}$ , relevant only at higher energies (similar to trigonal lattice potentials [48]).

In general, our results imply functional control of the spin polarization and the spectral gap by experimental design of the interface properties, enriching and enhancing the range of applications of topological insulators.

*Acknowledgements.* This research was supported by NSF via grants DMR-1410741 and DMR-1151717.

- 
- [1] M. Z. Hasan and C. L. Kane, Rev. Mod. Phys. **82**, 3045 (2010).
  - [2] X.L. Qi and S.C. Zhang, Rev. Mod. Phys. **83**, 1057 (2011).
  - [3] B. A. Bernevig and T. L. Hughes, *Topological Insulators and Topological Superconductors*. (Princeton University Press, Princeton, New Jersey, 2013).
  - [4] Q. Zhang et al., *ACS nano* **6**, 2345 (2012).
  - [5] M.H. Berntsen, et al., Phys. Rev. B, **88**, 195132 (2013).
  - [6] R. Yoshimi, et al., Nat. Mater. **13**, 253 (2014).
  - [7] L. Fu and C. L. Kane, Phys. Rev. Lett. **9**, 096407 (2008).
  - [8] P. Zareapour, et al., Nat. Commun. **3**, 1056 (2012).
  - [9] F. Qu, et al., Sci. Rep. **2**, 339 (2012).
  - [10] Y. Fan et al., Nat. Mater. **13**, 699–704 (2014).

- [11] A. R. Melnik *et al.*, Nature **511**, 449–451 (2014).
- [12] A. A. Burkov and D. G. Hawthorn, Phys. Rev. Lett. **105**, 066802 (2010).
- [13] S. Raghu *et al.*, Phys. Rev. Lett. **104**, 116401 (2010).
- [14] D. Pesin and A. H. MacDonald, Nat. Mater. **11**, 409 (2012).
- [15] P. Ghaemi and R. S. K. Mong, and J. E. Moore, Phys. Rev. Lett. **105**, 166603 (2010).
- [16] J. Alicea, Rep. Prog. Phys. **75**, 076501 (2012).
- [17] Z-H. Pan, *et al.*, Phys. Rev. Lett. **106**, 257004 (2011).
- [18] K. Miyamoto, *et al.*, Phys. Rev. Lett. **109**, 166802 (2011).
- [19] P. G. Silvestrov, P. W. Brouwer, and E. G. Mishchenko, Phys. Rev. B **86**, 075302 (2012).
- [20] J. W. Villanova and K. Park Phys. Rev. B, **93**, 085122 (2016).
- [21] F. Zhang, C. L. Kane and E. J. Mele, Phys. Rev. B **86**, 081303 (2012).
- [22] J. H. Bardarson and J. E Moore, Rep. Prog. Phys, **76**, 056501, (2013).
- [23] A. A. Zyuzin, M. D. Hook, and A. A. Burkov, Phys. Rev. B **24**, 245428 (2011).
- [24] H. Zhang, *et al.*, Nature Phys. **5**, 438 (2009).
- [25] J. E. Moore and L. Balents, Phys. Rev. B **75**, 121306 (2007).
- [26] C.-X. Liu, *et al.*, Phys. Rev. B **82**, 045122 (2010).
- [27] B.A. Volkov and O.A. Pankratov, JETP Lett. **42**, 178 (1985).
- [28] L. Isaev, G. Ortiz and I. Vekhter, Phys. Rev. B **20**, 205423 (2015).
- [29] V. V. Enaldiev, I. V. Zagorodnev, and V. A. Volkov, JETP Lett. **101**, 89 (2015).
- [30] G. Bester and A. Zunger, Phys. Rev. B **71**, 045318 (2005).
- [31] O. Krebs *et al.*, Phys. Rev. Lett. **80**, 5770 (1998).
- [32] See supplementary material.
- [33] M. Altarelli, Phys. Rev. B **28**, 842 (1983).
- [34] L. G. Gerchikov and A. V. Subashiev, phys. stat. sol. (b) **160**, 443 (1990).
- [35] G. Y. Wu and T. C. McGill, Appl. Phys. Lett. **47**, 634 (1985).
- [36] J. N. Schulman, and Y.-C. Chang, Phys. Rev. B **33**, 2594 (1986).
- [37] N. A. Cade, J. Phys. C: Solid State Phys. **18**, 5135 (1985).
- [38] The numerical results are obtained using the parameters for Bi<sub>2</sub>Se<sub>3</sub> from Ref. 26:  $A_1 = 2.26 \text{ eV}\text{\AA}$ ,  $A_2 = 3.33 \text{ eV}\text{\AA}$ ,  $B_1 = -6.86 \text{ eV}\text{\AA}^2$ ,  $B_2 = -44.5 \text{ eV}\text{\AA}^2$ , and  $M = -m = 0.28 \text{ eV}$ .
- [39] The  $v_4$  term is disallowed by rotational symmetry of the [111] face, but would immediately appear at any surface that does not preserve the full rotations, such as [001] or [100], see [19, 20]
- [40] C. H. Li, *et al.*, Nat. Nano **9**, 218 (2014).
- [41] A. Dankert, *et al.*, Nano Lett. **15**, 7976 (2015).
- [42] J. Tian *et al.*, Sci. Rep. **5**, 14293 (2015).
- [43] I. Zeljkovic *et al.*, Nat. Nano **10**, 849 (2015).
- [44] Y. Okada *et al.*, Nat. Commun. **3** 1158 (2012).
- [45] A. A. Burkov, and L. Balents, Phys. Rev. Lett. **12**, 127205 (2011).
- [46] W. Luo and XL. Qi, Phys. Rev. B **87**, 085431 (2013).
- [47] J. Zhang, C. Triola and E. Rossi, Phys. Rev. Lett. **112**, 096802 (2014).
- [48] L. Fu, Phys. Rev. Lett. **103** 266801 (2009).
- [49] We note that neglecting the second derivative,  $p_z^2 = -\partial_z^2$ , in Eq. (4) and allowing for a discontinuity in  $\Psi(\mathbf{r}, z)$  at the topological boundary as in Ref. [21] gives results qualitatively different from ours.